Hydrodynamics, Mass Transfer, and Photocatalytic Phenol Selective Oxidation Reaction Kinetics in a Fixed TiO_2 Microreactor

Matic Krivec
Electronic Ceramics, Institute "Jožef Stefan", Jamova cesta 39, Ljubljana 1000, Slovenia

Jožef Stefan International Postgraduate School, Jamova cesta 39, Ljubljana 1000, Slovenia

Andrej Pohar
Laboratory of Catalysis and Chemical Reaction Engineering, National Institute of Chemistry, Hajdrihova 19, Ljubljana 1000, Slovenia

Blaž Likozar
Laboratory of Catalysis and Chemical Reaction Engineering, National Institute of Chemistry, Hajdrihova 19, Ljubljana 1000, Slovenia

Faculty of Chemistry and Chemical Technology, University Ljubljana, Aškerčeva 5, Ljubljana 1000, Slovenia

Goran Dražić
Electronic Ceramics, Institute "Jožef Stefan", Jamova cesta 39, Ljubljana 1000, Slovenia

Jožef Stefan International Postgraduate School, Jamova cesta 39, Ljubljana 1000, Slovenia

Laboratory for Materials Chemistry, National Institute of Chemistry, Hajdrihova 19, Ljubljana 1000, Slovenia

DOI 10.1002/aic.14648
Published online October 16, 2014 in Wiley Online Library (wileyonlinelibrary.com)

Photocatalytic phenol dissociation was studied in a microreactor, with a TiO_2 layer immobilized on the reactor inner walls. Experiments were conducted for various residence times, initial concentrations, pH values, and UV light irradiation intensities. The intermediates and products (catechol, hydroquinone, and resorcinol) were quantitatively investigated to determine the predominant reaction pathways for the investigated anatase catalyst. A three-dimensional mathematical model was used to simulate the heterogeneous photocatalysis reaction conditions with Langmuir–Hinshelwood mechanism, considering the adsorption/desorption thermodynamic equilibria, and for kinetic parameter estimation via regression analysis. The effectiveness factor, Thiele modulus, and the correction function were calculated to determine the pore diffusion effects. The value of pH had the dramatic effect of lowering the reaction rate due to the competitive adsorption of hydroxide ions and protons on the catalyst surface. A phenol conversion of 79.5% was achieved at the residence time of 7.22 min, but without total mineralization. © 2014 American Institute of Chemical Engineers
AIChE J, 61: 572–581, 2015
Keywords: photochemical reactions, microfluidics, mathematical modeling, mass transfer, catalysis

Introduction

In recent years, the interest in photocatalysis using semiconductors, and its various options of applicability, has grown exponentially all over the world. TiO_2 has proven to be one of the most appropriate photocatalysts due to its characteristic band-gap energy (3.0–3.2 eV), biological/chemical inertness, stability, and low price. Traditionally, photocatalysis with TiO_2 has been applied as an alternative method to remediate and degrade the hazardous chemicals from air, soil, and water.[1,2] Conversely, TiO_2-based technology can be successfully applied as a selective synthetic route for a wide range of organic molecules, used in the food, pharmaceutical, and cosmetic industries.[3] These reactions usually take place in a liquid environment (e.g., water) with the TiO_2 particles in the form of dispersed powders, which enables a uniform distribution of the catalyst and a high photocatalytic surface-to-volume ratio.[4] However, the nanoscale TiO_2 particles in the suspensions have to be separated from the reaction products and recycled, which is an expensive and time-consuming process. Furthermore, the strong absorbing properties of the suspended nanoparticles and organic molecules limit the penetration depth of the UV light, and therefore prevent an efficient, industrial scale-up process. The immobilization of the TiO_2 photocatalyst to a fixed

Correspondence concerning this article should be addressed to A. Pohar at andrej.pohar@ki.si.

© 2014 American Institute of Chemical Engineers

surface represents a suitable way to remove the aforementioned restrictions, although this configuration may generate a unique problem of a low interfacial surface area, which can consequently lead to mass-transfer flux limitations.[5]

Microtechnology is an area that is rapidly evolving and growing in many areas of application. In the past two decades, microstructured process devices used to execute chemical reactions have shown impressive progress in terms of the intensification of the aforementioned operations.[6,7] The feasibility of laminar flow, short molecular diffusion distances, large surface-to-volume ratios, and efficient heat transfer are some of the many characteristics that give the processes in microreactors an advantage over those performed in conventional reactors.[8] Moreover, focusing on photochemical reactions, a high homogeneity of surface illumination and an excellent light penetration throughout most of the reactor volume provides a good distribution of photons throughout the reactor.[9] The catalytic microstructured reactors with an immobilized TiO_2 catalyst successfully exploit the aforementioned advantages and can be efficiently used for the degradation and chemical transformation of various organic chemicals, and even for the selective cleavage of proteins and peptides.[10,11]

Phenol and its derivatives are hazardous, water-soluble compounds that represent a huge environmental and toxicological problem due to the wastewater release from a variety of industrial and domestic activities.[12] Although a complete mineralization of these chemicals with the use of photocatalytic TiO_2 has been widely investigated, much less attention has been paid to photocatalytic selective oxidation, and to the exploration of different parameters (flow rate, initial component concentration, pH, UV light intensity, etc.) affecting this process.[13]

Microreactor technology can thus be used for small scale, flexible water treatment or for large scale, specific pollutant removal by means of numbering up, but only provided that all the pertinent governing mechanisms are well described using the modeling for consequent intensification and optimization. In this regard, phenol and its reaction intermediates may be considered as suitable model compounds due to the existing literature data covering the mechanisms and kinetics of their degradation, on one hand,[14–23] and owing to them being one of the major environmental pollutants, on the other. Nonetheless, although the mechanism and kinetics of phenol degradation are rather complex, first-order kinetics[16,23] or Langmuir–Hinshelwood kinetics that do not consider the reaction intermediates[18,19,21] are often used, unorthodoxly obtaining phenol concentration-dependent reaction rate constants,[19,23] or applying only the initial phenol concentration in the denominator of the Langmuir–Hinshelwood expression.[21] An advanced approach includes either the consecutive Langmuir–Hinshelwood kinetics of intermediates,[14,20] or the competitive parallel reactions of phenol to reaction intermediates and carbon dioxide[15,17]; however, reacting species are still treated as lumped components. Moreira et al.[22] recently proposed a comprehensive reaction scheme, breaking down all the lumped intermediate components into individual species. Nevertheless, the same study circumvented the acknowledgment of other mechanisms, governing the process, such as fluid mechanics, and (internal and external) mass transfer, taking into account only concomitantly with simplified kinetics,[20] while process parameters such as the pH and irradiation intensity were disregarded. Although the Langmuir–Hinshelwood mechanism for phenol photodegradation had been questioned in the past, it is widely accepted in more recent literature.[14,19–22] The best degradation models are based on Langmuir–Hinshelwood kinetics and have been built on very accurate analysis of both phenol and its most abundant by-products.[20]

In view of this, the present investigation explores these governing mechanisms, that is, fluid mechanics, transport phenomena, and chemical kinetics, for the degradation of phenol in a microreactor using photocatalysis, examining the effects of process parameters such as volumetric flow rate, irradiation intensity, concentration, pH and others, both in terms of measurements as well as the description by proposing a suitable photocatalytic process model.

Experimental

Materials and preparation

Titanium foil (Ti, 99.6 wt %, annealed, with the dimensions of $25 \times 25 \times 1$ mm^3, Goodfellow Cambridge, Huntington, England), poly(methyl methacrylate) sheet (PMMA, Plexiglas grade, UV-transparent, with the dimensions of $25 \times 25 \times 2$ mm^3, Acrytech d.o.o., Ljubljana, Slovenia), fluorinated ethylene propylene tubing (technical grade, of appropriate length, with an internal diameter of 0.5 mm, Vici AG International, Schenkon, Switzerland), titanium (IV) chloride ($TiCl_4$, 99.9 wt %, Acros Organics, NJ), ethylene glycol (EG, 99.5 wt %, Carlo Erba Reagents, Val de Reuil, France), ammonium fluoride (NH_4F, reagent grade, Kemika d.d., Zagreb, Croatia) were used for the synthesis of the TiO_2 film and the fabrication of the microreactor, described below.

Phenol (99.9 wt %, Sigma–Aldrich Chemie GmbH, Steinheim, Germany), catechol (99.9 wt %, Sigma–Aldrich Chemie GmbH, Steinheim, Germany), resorcinol (99 wt %, ABCR GmbH & Co. KG, Karlsruhe, Germany), hydroquinone (99.9 wt %, Sigma–Aldrich Chemie GmbH, Steinheim, Germany), and acetonitrile (>99.9 wt %, hypergrade for LC–MS LiChrosolv®, Merck KGaA, Darmstadt, Germany) were used for the photocatalytic degradation measurements without further purification. Demineralized water was used to dissolve phenol, catechol, resorcinol, and hydroquinone prior to measurements, while the desired pH was adjusted using sodium hydroxide (>99 wt %, pro analysi, Merck KGaA, Darmstadt, Germany) and perchloric acid (70 wt %, Suprapur®, Merck KGaA, Darmstadt, Germany).

TiO_2 fixed-bed microreactor and photocatalyst features

A detailed description of the fabrication of the microreactor and the immobilization of the TiO_2 dual layer on its inner walls were described in our previous work.[24] In brief, a serpentine microchannel was engraved in a titanium foil using a high-precision computer numerically-controlled (CNC) milling machine. The inner walls of the microchannel were immobilized with a two-step synthesis. First, the titanium-based flow microreactor was anodized in the EG solution with a small portion of NH_4F (0.3 wt %) at 60 V for 3 h. Second, the anodized flow microreactor was hydrothermally treated at 75°C for 1 h in a Teflon-lined stainless-steel autoclave, filled with a water suspension of $TiCl_4$ (0.2 M). Third, the prepared flow microreactor was thermally treated at 400°C for 3 h, covered with UV-transparent Plexiglas, and sealed with epoxy glue. The whole fabricated device was mounted in a stainless-steel housing with four integrated UV-light-emitting diode (LED) diodes (Roithner Lasertechnik GmbH, Vienna, Austria) with the emission maximum at 365 nm. Any increase in

temperature inside the microreactor was considered insignificant due to the use of LED diodes.

The TiO_2 film was investigated with a focused-ion-beam workstation (Helios NanoLab 650, FEI, Hillsboro, OR), a transmission electron microscope (JEM-2010F, JEOL, Tokyo, Japan), and an x-ray diffractometer (X'Pert PRO MRD, PANalytical, Almelo, The Netherlands). The total integrated incident intensity between 290 and 390 nm was measured with a radiation meter (PCE-UV34 UVA/UVB, PCE Instruments, Hampshire, UK), at different distances from the source.

Photocatalytic degradation experiments and decomposition of phenol and intermediates

The decomposition of the possible intermediates was studied in separate experiments (prior to the experiments involving phenol) for the determination of the reaction pathways and kinetic parameters. The photocatalytic degradation of catechol was studied in an experiment conducted at neutral pH, in room-temperature conditions (22°C), a UV intensity of 1.2 mW cm^{-1}, and an initial catechol concentration of 2.27×10^{-4} mol L^{-1}. In a typical experiment, the water solution of catechol was continuously pumped through the reactor at volumetric flow rates of 100, 80, 50, 20, and 10 μL min^{-1}, which correspond to the residence times of 0.72, 0.90, 1.44, 3.61, and 7.22 min, using a high-precision syringe pump (TSE Systems, Chesterfield, MO). For the determination of the significant reaction pathways, experiments involving catechol, hydroquinone, and resorcinol were conducted, in which 2.27×10^{-4} mol L^{-1} of each species was pumped through the microreactor under identical conditions as with the previous experiments.

The photocatalytic activity of the TiO_2-based flow microreactor was determined with the transformation of phenol. Before collecting the samples at an individual flow rate, 200 μL of the phenol solution was pumped through the reactor to clean any main and side products that were present from the previous experiment. The impact of the reaction conditions on the photocatalytic degradation of phenol was investigated by using four different initial concentrations of phenol (6.08×10^{-5}, 1.17×10^{-4}, 2.60×10^{-4}, and 5.31×10^{-4} mol L^{-1}), three different pH values (2.4, 6.0, and 10.5), and UV intensities (1.2, 5.0, 8.6, and 9.3 mW cm^{-2}) (ML-103B, MX Power, Shenzhen, China) at the volumetric flow rates of 100, 80, 50, 20, and 10 μL min^{-1}.

The transition from transient to steady-state operation of the system was characterized with a determination of the phenol concentration after different times of sampling. In brief, the water solution of phenol (2.60×10^{-4} mol L^{-1}) was continuously pumped through the reactor at three different volumetric flow rates (25, 50, and 75 μL min^{-1}). In contrast to the photocatalytic degradation experiments, samples were collected immediately ($t = 0$ min) after turning on the syringe pump, and after different time intervals, depending on the volumetric flow rate, that is at 75 μL min^{-1} (3, 6, and 9 min), 50 μL min^{-1} (10, 15, and 20 min), and 25 μL min^{-1} (15, 25, and 45 min). Before starting an individual experiment, the reactor was thoroughly washed with deionized water. An additional experiment was conducted in the dark to determine the phenol desorption–adsorption equilibrium on the surface of the photocatalyst.

The 750-μL aliquots of the reactants, products, and intermediates were collected and analyzed with a high-performance liquid-chromatography apparatus (HPLC, Agilent 1100 Series, Agilent, Santa Clara, CA), equipped with a UV–Vis detector (G1315A), and a solvent delivery pump (G1312A). The isocratic elution at a constant flow rate of 1 mL min^{-1} was used in a Phenomenex (Torrance, CA) Synergi^{TM} 4 μ Hydro-RP 80 Å analytical column (250×4.6 mm^2, 4-μm packing), using Milli-Q water and acetonitrile mixture [70:30 (vol/vol)] as a solvent. Total carbon (TC), total organic carbon (TOC), and inorganic carbon (IC) were determined using a Rosemount Analytical Dohrmann DC-190 (Irvine, CA). The concentrations of phenol, intermediates, and products were analyzed at 254 nm. Under these conditions, phenol, hydroquinone, catechol, and resorcinol with the retention times of 9.95, 5.68, 5.17, and 4.09 min, correspondingly, could be separated within 11 min.

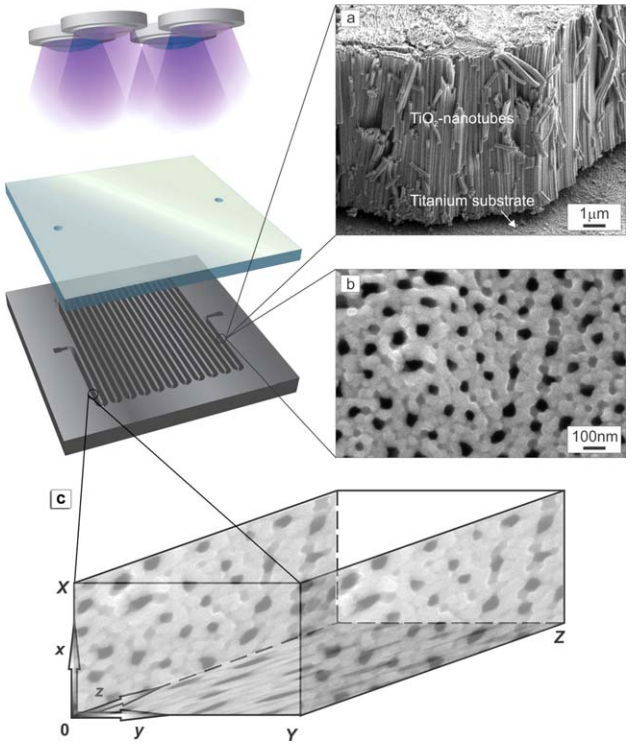

Figure 1. A scheme of the microreactor with two SEM micrographs: (a) a side-view of an immobilized TiO_2 nanoparticle/nanotube dual layer, (b) its top-view with small TiO_2 pores, and (c) the scheme of the microchannel with the catalytic anatase layer on the side and bottom walls.

[Color figure can be viewed in the online issue, which is available at wileyonlinelibrary.com.]

Theory

The fluid mechanics within the microreactor were described by the mass continuity equation (Eq. 1) combined with Navier–Stokes equations, simplified for the incompressible flow of Newtonian fluids (Eq. 2), utilizing the no-slip boundary conditions on the microreactor walls and the fully developed laminar-channel-flow boundary condition at the microreactor entrance (Eq. 3). v, ρ, p, μ, x, y, z, Q, and d represent the velocity, density, pressure, dynamic viscosity, microreactor height, width, and length coordinates (with the maximum values of X, Y, and Z), the volumetric flow rate, and hydraulic diameter, respectively. The microreactor setup can be seen on Figure 1. Calculations were executed for $z > Z$, while predictions were obtained at $z = Z$

$$\nabla \cdot v = 0 \tag{1}$$

$$\rho(v \cdot \nabla v) = -\nabla p + \mu \nabla^2 v \tag{2}$$

$$v = (0,0,0) \forall ((x=0 \vee x=X) \vee (y=0 \vee y=Y));$$
$$0 = -\frac{128Q}{\pi d^4} + \left(\frac{\partial^2 v}{\partial x^2} + \frac{\partial^2 v}{\partial y^2}\right) \forall (z=0) \tag{3}$$

The component balances for the individual species can be written using Eq. 4, with the catalytic reaction occurring on three microreactor walls (Eq. 5), while the reaction rates can be defined by Eq. 6, the $\pm$ sign accounting for the reactants/intermediates/products. C_i, D_i, r_i, k_i, K_i, t, I, and n represent the concentration, diffusivity, reaction rate, reaction rate constant, and Langmuir adsorption constant of the component i, and the time, relative incident irradiance, and irradiance-dependence exponent

$$\frac{\partial C_i}{\partial t} = -v \cdot \nabla C_i - D_i \nabla^2 C_i \tag{4}$$

$$-D_i \frac{\partial C_i}{\partial x} = r_i \forall (y=0 \vee y=Y);$$
$$-D_i \frac{\partial C_i}{\partial y} = r_i \forall (x=0); \; -D_i \frac{\partial C_i}{\partial y} = 0 \forall (x=X) \tag{5}$$

$$r_i = \frac{\sum_{j=1}^{J} (\pm \eta_j k_j K_j C_j)}{1 + \sum_{k=1}^{K} K_k C_k} I^n \tag{6}$$

Whereas, the effects of the volumetric flow rate and concentration are inherently accounted for in the model of Eqs. 1–6, the irradiance implicitly pertains to Langmuir–Hinshelwood kinetics (Eq. 6), which may be claimed for pH as well, as hydroxide ions and protons competitively adsorb on the catalyst surface (K_k) and reduce the reaction rate.[20] The reaction rate in a pore can be conveniently expressed by its rate under surface conditions multiplied by the effectiveness factor.[25,26] The effectiveness factor (η_i; Eq. 7) considers the internal mass transfer, which accounts for the difference between the global and intrinsic reaction rates, linearly reducing the reaction rate constant. The effectiveness factor should be considered when pore diffusion effects need to be taken into consideration.[27]

The evaluation of the effectiveness factor requires a calculation of the Thiele modulus ($M_{T,i}$), which is a dimensionless number that describes the relationship between the rate of diffusion and the reaction in a porous catalyst. Molecular diffusion in pores was presumed due to utilization of liquid contrary to gas phase (Knudsen diffusion). For Langmuir–Hinshelwood kinetics, the general modulus can be calculated with Eq. 8. The correction function (f_i) is used to counter the errors associated with the first-order approximation methods (Eq. 9), where $m_{eff,i}$ is the effective reaction order for the Langmuir rate equations (Eq. 10)[26]

$$\eta_i = f_i \frac{\tanh(M_{T,i})}{M_{T,i}} \tag{7}$$

$$M_{T,i} = L\sqrt{\frac{k_i}{2D_i}} \frac{K_i C_i}{1 + K_i C_i} (K_i C_i - \ln(1 + K_i C_i))^{-\frac{1}{2}} \tag{8}$$

$$f_i = \left(1 + \frac{\sqrt{1/2}}{\frac{1}{2M_{T,i}^2} + 2M_{T,i}^2}\right)^{\frac{1}{2}(1-m_{eff,i})^2} \tag{9}$$

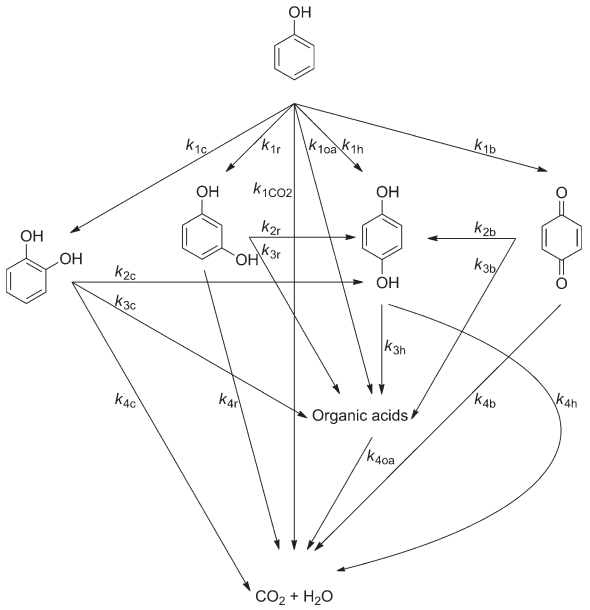

Figure 2. Detailed series–parallel reaction network for the photodegradation of phenol on a TiO_2 catalyst; index 1 represents the reactions of phenol (p) to catechol (c), resorcinol (r), hydroquinone (h), benzoquinone (b), organic acids (oa), and CO_2 (CO2), index 2, the reactions to hydroquinone, index 3, the reactions to organic acids, and index 4, the mineralization to CO_2.

$$m_{eff,i} = \frac{1}{1 + K_i C_i} \tag{10}$$

The binary liquid diffusion coefficients (Eq. 11) were calculated through the correlation provided by Siddiqi and Lucas,[28] which is based on the viscosity of the solvent (μ_b) and the molar volumes of the solute (V_i) and solvent (V_b) at their normal boiling points

$$D_i = 9.89 \times 10^{-8} T \frac{V_b^{0.265}}{\mu_b^{0.907} V_i^{0.45}} \tag{11}$$

The mass continuity equations were solved using the finite-difference approach in MATLAB. For the calculation of the velocity field, the semi-implicit method for pressure linked equations algorithm was used. Grid independency was assured.

One of the best reaction schemes was proposed by Moreira et al.,[22] updated in this study by the addition of resorcinol, and represented in Figure 2. As is evident from the figure, phenol can mineralize directly or via acid, benzenediol, or benzenedion intermediates. The latter two also allow for either direct mineralization or indirect via acidic intermediates, while the reaction scheme is characterized by benzenediol isomerization to hydroquinone as well.

Results and Discussion

Microreactor and catalyst characterization

Figure 1 shows the design of the TiO_2-based microreactor. A 390-mm-long, 0.5-mm-wide, and 0.36-mm-deep serpentine microchannel was immobilized with an approximately 10-μm-thick TiO_2 nanoparticle/nanotube film. The scanning

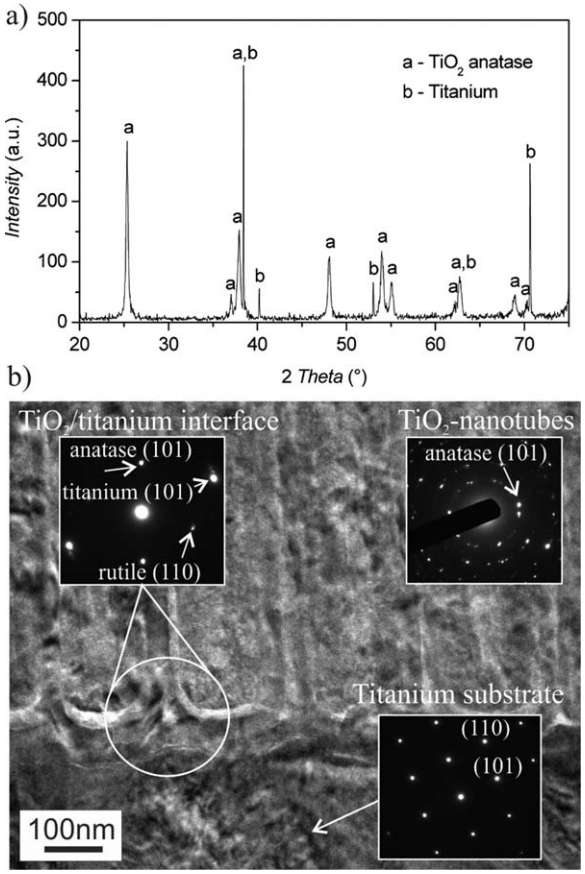

Figure 3. Determination of the crystal phases in the TiO_2 nanoparticle/nanotube dual layer: (a) x-ray diffraction (XRD) pattern and (b) SAED patterns for different regions of catalyst sample.

electron microscopy (SEM) micrograph in Figure 1 reveals the surface structure of the film, which consists of nanotubes with an average diameter of 100 nm that are surrounded and covered with an additional thin layer of small TiO_2 nanoparticles. The additional TiO_2 nanoparticles were introduced to the surface of the anodized nanostructures to increase the overall catalytic surface area. Our previous results[24] had shown that the photocatalytic activity increased significantly when the additional thin layer of TiO_2 nanoparticles was present on the TiO_2-nanotube film. The x-ray diffraction pattern in Figure 3a shows the presence of single-phase anatase with some additional peaks that correspond to the titanium substrate. Selected-area electron diffraction patterns in Figure 3b indicate the presence of a rutile phase at the TiO_2/titanium interface, while the scaffold and the body of the nanotubes consist of pure anatase-phase crystals. The prepared microreactor has a considerably smaller reactor volume (70 μL), a relatively high catalytic surface-to-volume ratio (6777 $m^2\ m^{-3}$) and a high temperature stability (0.3 K h^{-1}) under long-term operating conditions.[24] The highest Reynolds number under the experimental conditions of the highest flow rate of 100 μL min^{-1} was less than 4, which indicates that the flow was highly laminar, which justified the utilization of Eqs. 2 and 3 for laminar flow.

PMMA covered only the top wall of the microchannel, whereas the reaction with the radicals only took place on the TiO_2-coated walls. It is expected that the radicals were not long-lived and would not be able to attack the top PMMA wall. It was also assessed that the radicals did not attack the epoxy glue as no by-products were detected with HPLC. During the course of experimentation, contaminant products, if present, would have been identified.

External/internal mass transfer

The calculated Thiele moduli of the components in the solution were less than 6×10^{-4} in all cases, which implies that the internal diffusion phenomenon can be considered negligible. The effectiveness factors, required for the calculations of the reaction rates (Eq. 6) were 1, correct to the seventh decimal place. This confirms that the internal mass transfer does not play a role in the reaction mechanism, and that the determined reaction rates are in fact intrinsic. The reactions, thus, take place both on the surface of the catalyst and in its pores. As four radiation sources were positioned on top of the microreactor in the direct vicinity of the microchannel, an almost parallel light penetration into the pores from all angles was presumed (the pore diameter is wide enough to grant unhindered flux), and moreover, the pores are relatively straight (Figure 1a) with a tortuosity factor extremely close to unity.

The calculated diffusion coefficients were 7.05×10^{-10} $m^2\ s^{-1}$ for phenol, 6.85×10^{-10} $m^2\ s^{-1}$ for hydroquinone, 6.85×10^{-10} $m^2\ s^{-1}$ for catechol, and 1.07×10^{-9} $m^2\ s^{-1}$ for organic acids (the average for formic and acetic acid). The diffusion coefficient of dissolved CO_2 was taken as 1.60×10^{-9} $m^2\ s^{-1}$. The Péclet number for mass transfer is a dimensionless number that compares the rate of the advection of a species to its rate of diffusion. At the lowest experimental flow rate of 10 μL min^{-1}, the Péclet numbers of all the species were over 240, which indicate that the role of convection is dominant over diffusional transport and that the effect of diffusion in the way of convection is negligible, but was considered nonetheless.[29]

Figure 4 illustrates the influence of the increase/decrease of the phenol diffusion coefficient by one order of magnitude (e.g., on use of different temperature or solvent). Figure 4a presents the isosurface plot of the phenol concentration profile under for the case of 10 times lower phenol diffusion coefficient. There is a high diversity of phenol concentration across the microchannel cross-section, which is less pronounced in the case of the original phenol diffusion coefficient (Figure 4b). At the conditions of 10 times faster phenol diffusion (Figure 4c), its concentration is almost homogenous across the microchannel cross-section.

Regression of intrinsic kinetic parameters, reaction kinetics, and rate

The photocatalytic degradation of phenol in water starts with the formation of a phenoxy radical from the reaction between phenol and photocatalytically generated $OH^{\bullet}$. The phenoxy radical is in resonance with two radical structures in the ortho and para positions. They can react with OH^- and form di-hydroxylated side products, such as catechol and hydroquinone. In the next step, ortho and para benzoquinones are formed either by the reaction of catechol and hydroquinone with OH^-, their oxidation with photogenerated holes in TiO_2 or by direct oxidation with dissolved oxygen in water. Further oxidation leads to the opening of the benzene structure and the formation of smaller oxygen-contained aliphatic compounds and ends with the final

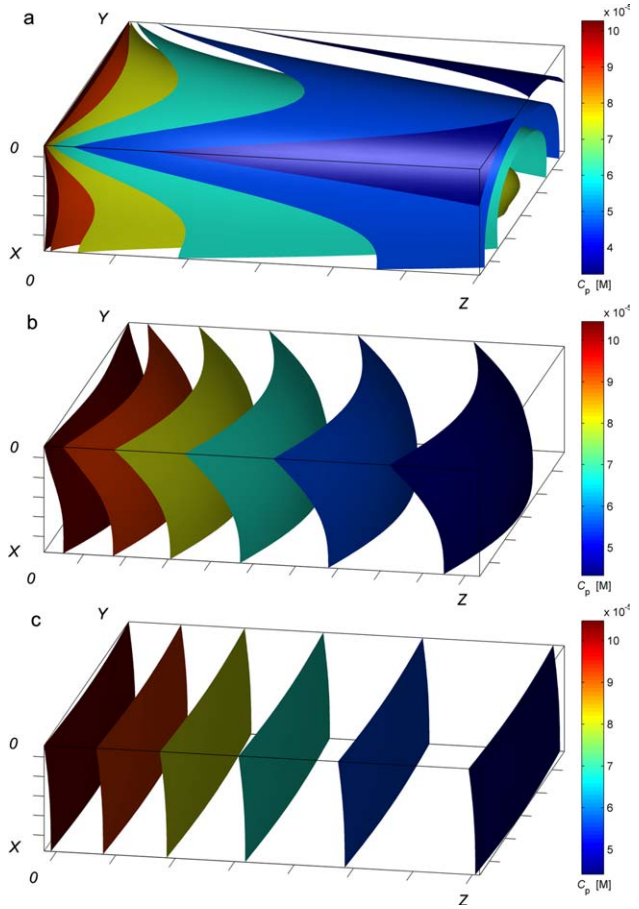

Figure 4. The effect of phenol diffusion coefficient (isosurface plot): (a) 10 times lower diffusion coefficient, (b) original diffusion coefficient, and (c) 10 times higher diffusion coefficient at the flow rate of 10 μL min^{-1} and initial phenol concentration of 1.17 × 10^{-4}.

[Color figure can be viewed in the online issue, which is available at wileyonlinelibrary.com.]

mineralization to CO_2 and H_2O.[30] Nonetheless, Moreira et al.[22] and other studies showed that several characteristics of TiO_2 material (structure, morphology, distribution of phases, etc.) largely influence the intrinsic kinetics and selectivity of a TiO_2-based catalyst for individual reactions in Figure 2 (e.g., phenol radical formation).

The relevant adsorption coefficients of the Langmuir–Hinshelwood kinetics (Eq. 6) were obtained from the work of Moreira et al.[22] The values for phenol (K_p), hydroquinone (K_h), catechol (K_c), and organic acids (K_{oa}; taken as the average value for acetic and formic acid) were 7.70 × 10^3 L mol^{-1}, 6.84 × 10^3 L mol^{-1}, and 6.05 × 10^3 L mol^{-1}, in the same order.

Regarding photocatalytic catechol degradation, the maximum conversion obtained at the smallest flow rate of 10 μL min^{-1} was 8.3%. HPLC analysis detected only catechol, while phenol, hydroquinone, benzoquinone, resorcinol, or benzoquinone were not identified, or were below the detection limit. This eliminates the reaction pathway leading from catechol to hydroquinone with the corresponding kinetic parameter k_{2c}. Furthermore, a TOC analysis revealed there was no increase in CO_2 presence in the product solution, excluding the mineralization pathway to CO_2 and H_2O, with the corresponding kinetic parameter k_{4c}, corresponding to a slow reaction rate for catechol mineralization, reported in literature.[22]

In the experiment involving catechol, hydroquinone, and resorcinol, the concentrations of hydroquinone and resorcinol did not exhibit any change for the various flow rates tested, within the margins of experimental uncertainty. Catechol, however, showed a similar concentration drop at lower flow rates, as was observed in the previous experiment. This excludes the possible transformation of resorcinol to hydroquinone (k_{2r}), its degradation to organic acids (k_{3r}), and mineralization (k_{4r}), during the residence times of the experiments. Similarly, hydroquinone did not degrade in the time of the experiment, eliminating the reaction pathway toward organic acids (k_{3h}) and mineralization (k_{4h}) for the studied catalyst.

This degradation mechanism and the reaction pathway of phenol decomposition, involving only hydroquinone as the reaction intermediate, correlates well to the research performed by Wang et al.,[31] who studied the effect of crystallite size and crystallinity of anatase nanoparticles on the photodegradation of phenol. The authors found that crystallinity had a negligible effect on phenol photodegradation and the evolution of the intermediates, whereas the crystallite size had a profound effect on the photocatalytic reaction pathways. They showed that the production of benzoquinone is completely suppressed in the case of the catalysts containing large anatase nanoparticles, while a significant evolution of hydroquinone takes place. The largest anatase nanoparticles in their work, which also gave the highest hydroquinone yield, were 26.8 nm. The anatase nanoparticle sizes, determined from the XRD pattern of the TiO_2 catalyst used in the present study (Figure 3a), calculated by the Scherrer equation were 24–110 nm, which explains the photodegradation of phenol to hydroquinone.

The authors[31] also observed hydroquinone accumulation for all the studied anatase catalysts. Furthermore, they showed that the selective oxidation of phenol to catechol is very slow, that the decomposition of phenolic compounds is faster than direct phenol decomposition, that phenol and its phenolic derivatives convert to CO_2 only after prolonged irradiation periods, and that the selective oxidation of phenol to catechol is very slow. Although the reasons for the evolution of different intermediates have been revealed, the underlying mechanisms have yet to be discovered.

The kinetics of catechol degradation to organic acids was determined with regression analysis, considering the results from the catechol experiments as well as the results from the experiments involving catechol, hydroquinone, and resorcinol. The determined kinetic constant for the transformation of catechol to organic acids (k_{3c}) was 6.72 × 10^{-9} mol m^{-2} s^{-1}. Figure 5 presents the experimental data and model results for catechol degradation during the residence time of the experiment, where c represents the catechol and ao represents the lumped organic acids (acetic and formic). The concentration of the organic acids was calculated through the stoichiometric relationship due to the obtained negligible extent of mineralization and is presented as the average value across the microchannel cross-section. The isosurface plot of the catechol concentration for 10 μL min^{-1} is presented in Figure 6.

During the experiments concerning the photocatalytic degradation of phenol only hydroquinone was detected, while catechol, resorcinol, and benzoquinone were not, or were below the detection limit. The appropriate reaction pathways

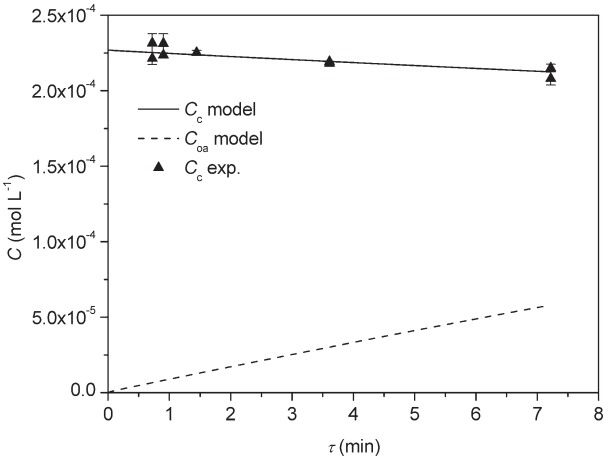

Figure 5. The experimental and model results (at microreactor exit, $z = Z$) of photocatalytic catechol degradation for different residence times (τ) (various utilized volumetric flow rates); C_c represents catechol concentration, while C_{ao} represents the organic acids' concentration.

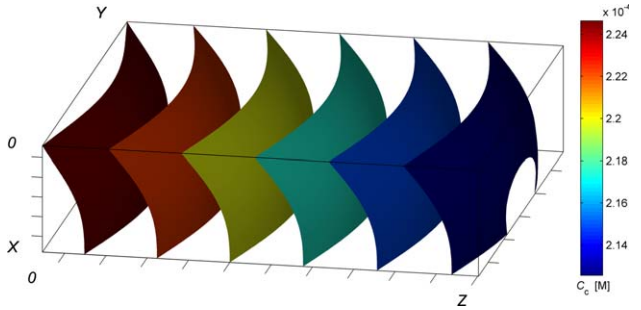

Figure 6. The isosurface plot of the concentration of catechol at 10 μL min^{-1} along microreactor.

[Color figure can be viewed in the online issue, which is available at wileyonlinelibrary.com.]

(with the kinetic constants k_{1c}, k_{1r}, and k_{1b}) were therefore excluded from the reaction scheme. As benzoquinone was never present in the system, its decomposition reaction constants k_{2b}, k_{3b}, and k_{4b} were not subject to regression analysis and were not evaluated. TC, TOC, and IC analyses showed that there was no increased CO_2 presence in the solution, eliminating the reaction pathways with the corresponding reaction constants k_{1CO2} and k_{4oa}. The kinetic-parameter determination was performed for k_{1h} (phenol to hydroquinone) and k_{1oa} (phenol to organic acids). The values obtained for k_{1h} and k_{1oa} were 3.47×10^{-8} mol m^{-2} s^{-1} and 9.30×10^{-8} mol m^{-2} s^{-1}, respectively. The experimental and model results (average concentrations across the microchannel cross-section) are presented in Figure 7 for the case of 6.08×10^{-5} mol L^{-1} (a) and 1.17×10^{-4} mol L^{-1} (b) initial phenol concentrations. Phenol conversions for the longest microreactor residence time of 7.22 min were 79.5, 69.9, 54.2, and 38.8% for the 6.08×10^{-5}, 1.17×10^{-41}, 2.60×10^{-4}, and 5.31×10^{-4} mol L^{-1} initial phenol concentrations.

The initial rates of reaction were higher at smaller initial phenol concentrations that is, even though the concentration of phenol linearly increases the reaction rate according to Langmuir–Hinshelwood mechanism (Eq. 6, numerator term), the adsorption is strongly shifted toward adsorbed as opposed to desorbed species (Eq. 6, denominator term). Thus, at higher initial phenol concentrations, the quantity of phenol absorbed on the catalyst surface increases and suppresses OH^- radical formation.[21] This may be deducted from the employed adsorption constants and is valid not only for phenol, but for intermediates as well. The latter may also be considered as one of the main underlying mechanisms, responsible for the limited extent of mineralization. The removal of reaction intermediates and products is under batch operation largely facilitated by vigorous mixing, quenching of the evolved species, and in turn shifting the adsorption equilibrium toward desorption. This seems to be rather suppressed under laminar flow conditions at low Reynolds numbers. A relatively simple solution would in this case pose itself by the utilization of passive or active micromixers and continuous reactor elongation to allow for comparable residence times and terminal phenol conversions.

The occurrence of possible reverse reactions of CO_2 to CH_4, CH_2O, and CH_3OH was discarded. Although the mentioned reactions are possible, the resulting species would have been detected and TOC analysis also showed that there was no change in the TOC.

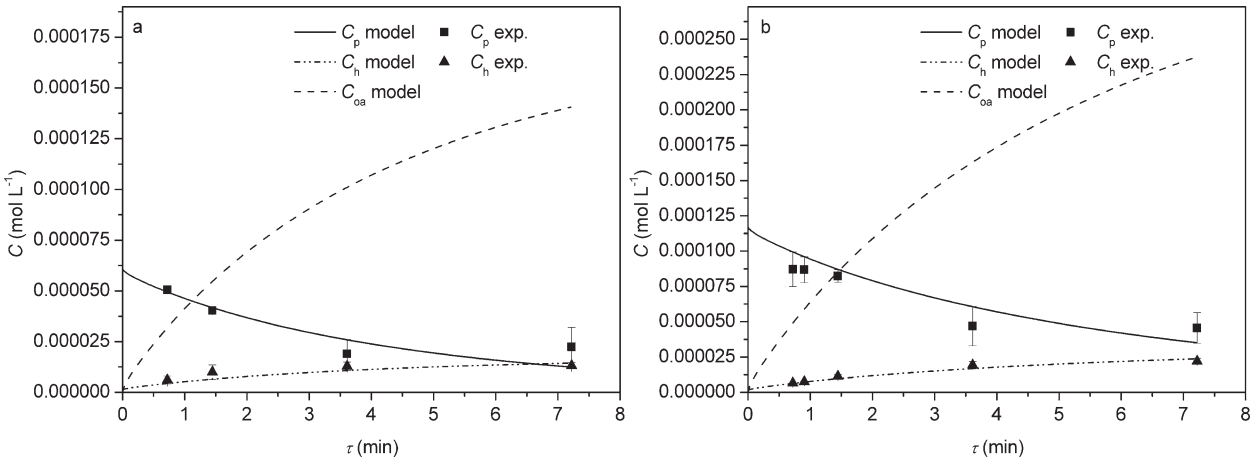

Figure 7. Photocatalytic degradation of phenol to hydroquinone and carboxylic acids at 6.08×10^{-5} mol L^{-1} (a) and 1.17×10^{-4} mol L^{-1} (b) initial phenol concentrations for various residence times (τ) corresponding to the different applied volumetric flow rates.

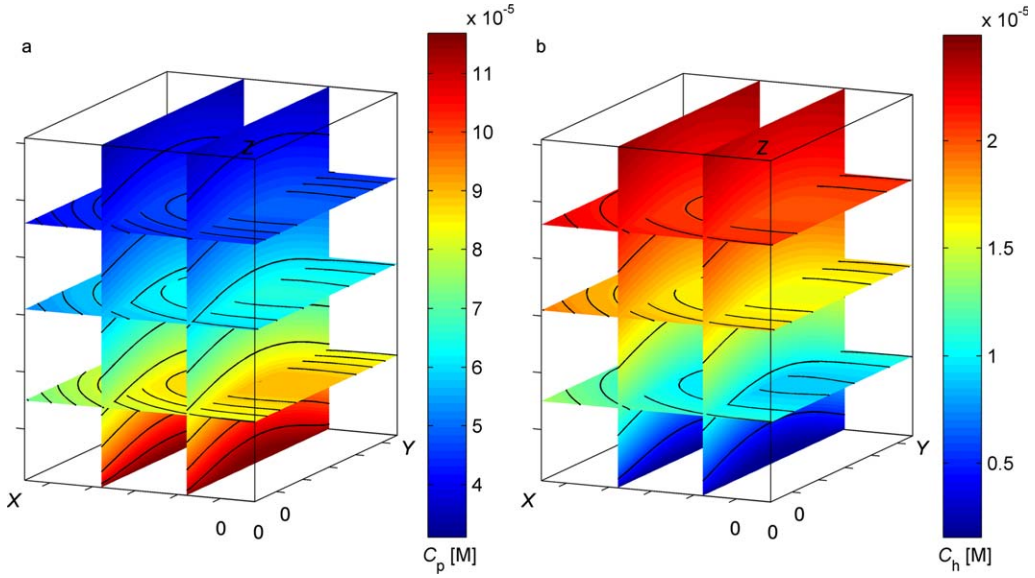

Figure 8. The concentration profile of phenol (p) and hydroquinone (h) under steady-state conditions at a flow rate of 10 μL min^{-1} and a 1.17 × 10^{-4} mol L^{-1} initial phenol concentration. The planes are positioned at 1/3 and 2/3 depth, and 1/4, 2/4, and 3/4 length.

[Color figure can be viewed in the online issue, which is available at wileyonlinelibrary.com.]

The concentration profiles of phenol and hydroquinone at a flow rate of 10 μL min^{-1} and a 1.17 × 10^{-4} mol L^{-1} initial phenol concentration are presented in Figure 8. It is clear that the concentration of phenol (p) is lower at the three catalytic walls, where the photocatalytic degradation takes place, and how the concentration of hydroquinone (h) is higher at the catalytically active walls. Diffusional transport in the directions parallel to the flow evens out the concentration difference, which pertains for phenol, hydroquinone, and organic acids alike.

Light intensity and pH

The results obtained from the experiments performed at different UV intensities (1.2, 5.0, 8.6, and 9.3 mW cm^{-2}) did not display any observable intensity-related effect on the reaction kinetics and are presented in Figure 9. Chowdhury et al.[21] showed that at much higher light intensities (e.g., 100 mW cm^{-2}), the value of the irradiance-dependence exponent n is approximately 2, which would explain the minute effect of light intensity at its much lower levels, as the derivative of quadratic dependence approaches zero on the utilization of no irradiance. Analogously was noted by Wang et al.[23] who obtained a rather poor dependence on irradiation that is the variation of irradiance power from 300 to 100 W (67% decrease) yielded only a 5% difference in the apparent reaction constant, which is within the margin of error. As the reaction rate was not dependent on light intensity, the irradiance term I^n was excluded from the rate equation (Eq. 6), and the kinetic parameters were presented under saturated light conditions. Drastically, lower light intensities would require the determination of light intensity dependent kinetic parameters, along with irradiance-dependent exponent n. Phenol did not decompose during the experiments conducted in the dark. Moreover, no decrease in phenol concentration was observed, when measurements were performed without UV irradiation, which would suggest that even though the thermodynamic equilibrium predominantly favors the adsorbed form as opposed to desorbed solvated species,[22] the catalytic surface to liquid volume in the microreactor was too small to provide noticeable phenol decrease solely due to phenol adsorption. Moreover, a low rate of adsorption may not be considered as the explanation for the lack of phenol degradation in the dark, as the majority of studies[14,15,17,20,22] point out the surface reaction as the rate-determining step, the latter being one of the essential suppositions to justify the validity of the formulated Langmuir–Hinshelwood mechanism.

The pH of a pollutant solution is an important parameter in a photocatalytic process. It determines the surface-charge properties of the photocatalyst and the interactions between the surface of the semiconductor and the organic molecules. The point of zero charge for titania was reported at pH 6.25, which means that the surface of TiO_2 is positively charged at lower pH and negatively charged at higher values.

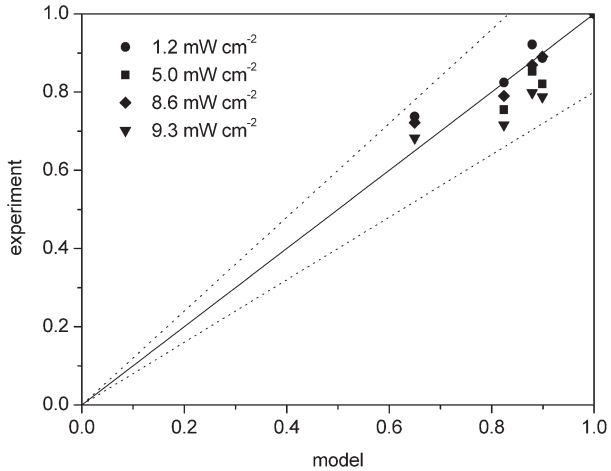

Figure 9. The parity plot comparing the experimental and model results for different light intensities. The dotted lines denote the 20% margin of error.

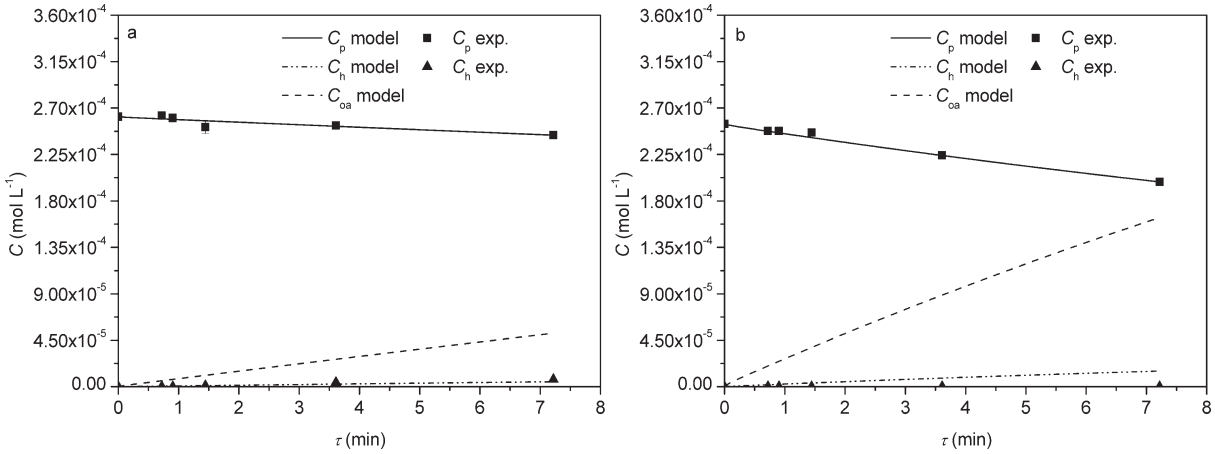

Figure 10. Photocatalytic degradation of phenol to hydroquinone and carboxylic acids at pH values of 2.4 (acidic) (a) and 10.5 (alkaline conditions) (b) for different residence times (τ).

Moreover, the high concentration of OH^- ions at higher pH values might generate a larger amount of oxidative hydroxyl radical species and, therefore, can enhance the activity of the photocatalytic process, which is not the case in the solutions with lower pH values. Conversely, OH^- ions create a strong repelling force with a negatively charged TiO_2 surface at higher pH values, which could be attributed to the decrease in the activity, observed in present study as well. Furthermore, a high concentration of OH^- ions prevents an effective penetration of UV irradiation to the catalytic surface.[32]

The effect of non-neutral pH was expressed as the competitive adsorption of hydroxide ions and protons on the catalyst surface, reducing the reaction rate by occupying the catalysts' active sites. The initial phenol concentration in the experiments was 2.60×10^{-4} mol L^{-1} and the UV intensity was 1.2 mW cm^{-2}. At a pH of 2.4, the corresponding concentrations of H^+ and OH^- ions were 3.98×10^{-3} mol L^{-1} and 2.15×10^{-12} mol L^{-1}, while for the pH of 10.5, the values for H^+ and OH^- ions were 3.16×10^{-11} mol L^{-1} and 3.16×10^{-4} mol L^{-1}. The Langmuir adsorption constants for the two ions were obtained by regression analysis of the experimentally obtained data and were 1.09×10^4 L mol^{-1} and 3.05×10^4 L mol^{-1} for H^+ and OH^-, respectively. A good agreement was obtained with the acquired constants at all pH values (Figure 10).

Transient operation

The transient experiments were performed at an irradiation intensity of 1.2 mW cm^{-2}, neutral pH, and various flow rates. Samples were collected prior to achieving steady-state conditions. The experimental concentrations were similar in all cases, within the experimental uncertainty, that is, the concentration of phenol increased basically as a step function, implying that the convection model for laminar flow [cumulative distribution function being defined as $F = 1–1/(4(t/\tau)^2)$] approached stepwise behavior. This means that the reactor approaches a plug-flow mode of operation at its end (exit effects may be considered responsible for parabolic profile flattening), with negligible longitudinal dispersion of the species in the solution due to axial dispersion, which had already been predicted by the calculation of the Péclet numbers and further verified with the transient experiments. The absence of any noticeable component breakthrough prior to $t = \tau$ implies not only the absence of any axial dispersion, but also back mixing due to the roughness (porosity) of the catalyst–liquid interface.

Conclusions

Photocatalytic phenol decomposition inside a fabricated microreactor system with TiO_2 immobilized on the microchannel walls was successfully performed with the highest conversion of 79.5% at for a residence time of 7.22 min, at 4.54×10^{-5} mol L^{-1} initial phenol concentration. The experiments showed that phenol decomposed to hydroquinone and organic acids, while hydroquinone did not decompose within the residence times of the experiments.

In this sense, hydroquinone, which is a commercially important chemical, was effectively produced in the photocatalytic microreactor system. TOC analysis showed that mineralization did not occur at any of the performed experimental conditions, a possible reason for this being the strong adsorption of species (reactants, intermediates, and products) and laminar flow conditions (species quenching). Catechol was the only intermediate which would decompose during the residence time of the experiment. Utilization of a microreactor system shows promise for the production of reaction intermediates, and can be precisely characterized and operated with the help of mathematical modeling. Furthermore, microreactors provide a suitable laboratory platform for kinetic studies.[33]

The results of this work showed selective phenol photodegradation to hydroquinone. Further research is required to explain the inherent mechanisms behind selective phenol degradation, which had been shown to be directly correlated to the size of the TiO_2 crystallites.[32]

Process modeling revealed the necessity to acknowledge transport phenomena in terms of external liquid mass transfer and pore diffusion to distinguish among the individual contributions to the overall degradation extent. Moreover, the analysis of reaction pathways showed that several reaction steps may be considered negligible, the latter being rather specific to catalyst characteristics, but the outlined methodology, nonetheless, still applies.

Literature Cited

1. Hoffmann MR, Martin ST, Choi W, Bahnemann DW. Environmental applications of semiconductor photocatalysis. *Chem Rev*. 1995;95: 69–96.

2. Fujishima A, Zhang X, Tryk DA. TiO_2 photocatalysis and related surface phenomena. *Surf Sci Rep*. 2008;63:515–582.
3. Palmisano G, Augugliaro V, Pagliaro M, Palmisano L. Photocatalysis: a promising route for 21st century organic chemistry. *Chem Commun*. 2007;33:3425–3437.
4. de Lasa H, Serrano B, Salaices M. *Photocatalytic Reaction Engineering*, 1st ed. New York: Springer Science+Business Media, 2005.
5. Ray AK, Beenackers AACM. Novel photocatalytic reactor for water purification. *AIChE J*. 1998;44:477–483.
6. Pohar A, Plazl I. Process intensification through microreactor application. *Chem Biochem Eng Q*. 2009;23:537–544.
7. Lindstrom H, Wootton R, Iles A. High surface area titania photocatalytic microfluidic reactors. *AIChE J*. 2007;53:695–702.
8. Jahnisch K, Hessel V, Lowe H, Baerns M. Chemistry in microstructured reactors. *Angew Chem Int Ed*. 2004;43:406–446.
9. Lu H, Schmidt MA, Jensen KF. A microfluidic electroporation device for cell lysis. *Lab Chip*. 2001;5:22–28.
10. Roberge DM, Ducry L, Bieler N, Cretton P, Zimmermann B. Microreactor technology: A revolution for the fine chemical and pharmaceutical industries? *Chem Eng Technol*. 2005;28:318–323.
11. Jones BJ, Vergne MJ, Bunk DM, Locascio LE, Hayes MA. Cleavage of peptides and proteins using light-generated radicals from titanium dioxide. *Anal Chem*. 2007;79:1327–1332.
12. Teh CM, Mohamed AR. Roles of titanium dioxide and ion-doped titanium dioxide on photocatalytic degradation of organic pollutants (phenolic compounds and dyes) in aqueous solutions: a review. *J Alloys Compd*. 2011;509:1648–1660.
13. Emeline AV, Zhang X, Murakami T, Fujishima A. Activity and selectivity of photocatalysts in photodegradation of phenols. *J Hazard Mater*. 2012;211:154–160.
14. Bellobono IR, Ascari F, Lagrasta C, Pinacci PL, Tozzi PM, Di Carlo MS, Simoncelli C. Kinetic modelling of photomineralization of phenol, as model molecule of aromatic micropollutants, and validation of a photochemical reactor based on photocatalytic membranes immobilizing titanium dioxide and promoting photocatalysts. *Fresen Environ Bull*. 2003;12:1536–1544.
15. Azevedo EB, Neto FRA, Dezotti M. TiO_2-photocatalyzed degradation of phenol in saline media: lumped kinetics, intermediates, and acute toxicity. *Appl Catal B*. 2004;54:165–173.
16. Tryba B, Morawski AW, Inagaki M, Toyoda M. The kinetics of phenol decomposition under UV irradiation with and without H_2O_2 on TiO_2, Fe–TiO_2 and Fe–C–TiO_2 photocatalysts. *Appl Catal B*. 2006; 63:215–221.
17. Azevedo EB, Tôrres AR, Aquino Neto FR, Dezotti M. TiO_2-photocatalyzed degradation of phenol in saline media in an annular reactor: hydrodynamics, lumped kinetics, intermediates, and acute toxicity. *Braz J Chem Eng*. 2009;26:75–87.
18. Montoya JF, Velásquez JA, Salvador P. The direct–indirect kinetic model in photocatalysis: a reanalysis of phenol and formic acid degradation rate dependence on photon flow and concentration in TiO_2 aqueous dispersions. *Appl Catal B*. 2009;88:50–58.
19. Sophyan I, Hafizah N, Jamal P. Immobilization of TiO_2 with cement: photocatalytic degradation of phenol. *Indian J Chem Technol*. 2011;18:263–270.
20. Vezzoli M, Martens WN, Bell JM. Investigation of phenol degradation: true reaction kinetics on fixed film titanium dioxide photocatalyst. *Appl Catal A Gen*. 2011;404:155–163.
21. Chowdhury P, Moreira J, Gomaa H, Ray AK. Visible-solar-light-driven photocatalytic degradation of phenol with dye-sensitized TiO_2: parametric and kinetic study. *Ind Eng Chem Res*. 2012;51:4523–4532.
22. Moreira J, Serrano B, Ortiz A, de Lasa H. A unified kinetic model for phenol photocatalytic degradation over TiO_2 photocatalysts. *Chem Eng Sci*. 2012;78:186–203.
23. Wang YH, Zhao JL, Liang Y. Degradation kinetics of phenol by a titanium dioxide photocatalyst coupled with a magnetic field. *React Kinet Mech Catal*. 2013;109:273–283.
24. Krivec M, Žagar K, Suhadolnik L, Čeh M, Dražić G. Highly efficient TiO_2-based microreactor for photocatalytic applications. *ACS Appl Mater Inf*. 2013;5:9088–9094.
25. Adagiri GA, Babagana G, Susu AA. Effectiveness factor for porous catalysts with specific exothermic and endothermic reactions under Langmuir-Hinshelwood kinetics. *IJRRAS*. 2012;13:716–739.
26. Thiele EW. Relation between catalytic activity and size of particle. *Ind Eng Chem*. 1939;31:916–920.
27. Hong J, Hecker W, Fletcher T. Predicting the effectiveness factor for mth order Langmuir rate equations in spherical coordinates. *ACS Symp Ser*. 1999;44:1011–1015.
28. Siddiqi MA, Lucas K. Correlations for prediction of diffusion in liquids. *Can J Chem Eng*. 1986;64:839–843.
29. Ungerböck B, Pohar A, Mayr T, Plazl I. Online oxygen measurements inside a microreactor with modeling of transport phenomena. *Microfluid Nanofluid*. 2013;14:565–574.
30. Grabowska E, Reszczyńska J, Zaleska A. Mechanism of phenol photodegradation in the presence of pure and modified-TiO_2: a review. *Water Res*. 2012;46:5453–5471.
31. Wang X, Sø L, Su R, Wendt S, Hald P, Mamakhel A, Yang C, Huang Y, Iversen BB, Besenbacher F. The influence of crystallite size and crystallinity of anatase nanoparticles on the photodegradation of phenol. *J Catal*. 2014;310:100–108.
32. Qamar M, Muneer M, Bahnemann D. Heterogeneous photocatalysed degradation of two selected pesticide derivatives, triclopyr and daminozid in aqueous suspensions of titanium dioxide. *J Environ Manage*. 2006;80:99–106.
33. Srinivasan R, Hsing IM, Berger PE, Jensen KF, Firebaugh SL, Schmidt MA, Harold MP, Lerou JJ. Micromachined reactors for catalytic partial oxidation reactions. *AIChE J*. 1997;43:3059–3069.

Manuscript received Feb. 17, 2014, and revision received Oct. 1, 2014.